Tenth U.S. National Conference on Earthquake Engineering
Frontiers of Earthquake Engineering
July 21-25, 2014
Anchorage, Alaska

UNCOVERING THE HETEROGENEITY OF SPATIAL LIFELINE SYSTEM INTERDEPENDENCIES

R. Paredes-Toro[1]*, L. Dueñas-Osorio[2], G. P. Cimellaro[3]

ABSTRACT

Lifeline systems are complex geographically distributed systems that are essential to the well-being of modern society and its response and recovery after natural disasters. For this reason, models of interdependent systems under a wide range of adverse events are emerging; nevertheless, it is not easy to assess the intensity of coupling across systems to make these models represent their actual behavior. Besides, this paper performs a systematic quantification of spatial interdependencies across multiple lifeline networks, including power, water, fixed telephone and internet systems, as representatives of modern smart infrastructures. The analysis expands a Kriging Aided Spatial Correlation Algorithm (KASCA) at the local scale that quantifies lifeline coupling strengths and provides a more explicit and reproducible formulation of the spatial approach. This is achieved by performing sensitivity analyses to best estimate the interdependence strengths across networks subjected to earthquakes across geographies that match predictions to field observations and local field features. The improved spatial analysis is applied for the first time to four systems in the context of the 2010 M_w 8.8 Chile Earthquake using utility restoration data sets and the results are compared with previous temporal and spatial analyses for subsets of the systems. Spatially varying coupling strengths resulting from this analysis are communicated via local correlation maps and synthesized into global correlation plots, which can point out interdependence directionality and length of coupling influence across lifeline systems. Addressing the spatial coupling behavior between networks is a crucial step towards modeling and robust quantification of the interdependencies between lifeline systems and associated facilities, while also supporting decision-making.

[1]Graduate Student, Dept. of Structural, Building & Geotechnical Engineering, Politecnico di Torino, Turin, ITALY.
[*]Research Intern, Dept. of Civil and Environmental Engineering, Rice University, Houston, TX 77005.
[2]Associate Professor, Dept. of Civil and Environmental Engineering, Rice University, Houston, TX 77005.
[3]Assistant Professor, Dept. of Structural, Building & Geotechnical Engineering, Politecnico di Torino, Turin, ITALY.

Paredes-Toro R, Dueñas-Osorio L, Cimellaro G P. Uncovering the Heterogeneity of Spatial Lifeline System Interdependencies. *Proceedings of the 10th National Conference in Earthquake Engineering*, Earthquake Engineering Research Institute, Anchorage, AK, 2014.

Tenth U.S. National Conference on Earthquake Engineering
Frontiers of Earthquake Engineering
July 21-25, 2014
Anchorage, Alaska

Uncovering the Heterogeneity of Spatial Lifeline System Interdependencies

R. Paredes-Toro[1*], L. Dueñas-Osorio[2], G.P. Cimellaro[3]

ABSTRACT

Lifeline systems are complex geographically distributed systems that are essential to the well-being of modern society and its response and recovery after natural disasters. For this reason, models of interdependent systems under a wide range of adverse events are emerging; nevertheless, it is not easy to assess the intensity of coupling across systems to make these models represent their actual behavior. Besides, this paper performs a systematic quantification of spatial interdependencies across multiple lifeline networks, including power, water, fixed telephone and internet systems, as representatives of modern smart infrastructures. The analysis expands a Kriging Aided Spatial Correlation Algorithm (KASCA) at the local scale that quantifies lifeline coupling strengths and provides a more explicit and reproducible formulation of the spatial approach. This is achieved by performing sensitivity analyses to best estimate the interdependence strengths across networks subjected to earthquakes across geographies that match predictions to field observations and local field features. The improved spatial analysis is applied for the first time to four systems in the context of the 2010 Mw 8.8 Chile Earthquake using utility restoration data sets and the results are compared with previous temporal and spatial analyses for subsets of the systems. Spatially varying coupling strengths resulting from this analysis are communicated via local correlation maps and synthesized into global correlation plots, which can point out interdependence directionality and length of coupling influence across lifeline systems. Addressing the spatial coupling behavior between networks is a crucial step towards modeling and robust quantification of the interdependencies between lifeline systems and associated facilities, while also supporting decision-making.

Introduction

Various lifeline system performance assessment models, either individually or coupled, continue to integrate post-event data for calibration purposes. Typically, they compare their numerical simulation and theoretical model predictions with field-reported network responses. For example, the Graphical Iterative Response Analysis of Flow Following Earthquakes (GIRAFFE), a model that performs hydraulic analysis on water networks subjected to seismic damage, has been calibrated with multiple data sets, including the 1994 Northridge earthquake [1]. More recently, a calibration of the Interdependence Fragility Algorithm (IFA), a general-purpose seismic

[1] Graduate Student, Dept. of Structural, Building & Geotechnical Engineering, Politecnico di Torino, Turin, ITALY.
[*] Research Intern, Dept. of Civil and Environmental Engineering, Rice University, Houston, TX 77005.
[2] Associate Professor, Dept. of Civil and Environmental Engineering, Rice University, Houston, TX 77005
[3] Assistant Professor, Dept. of Structural, Building & Geotechnical Engineering, Politecnico di Torino, Turin, ITALY.

Paredes-Toro R, Dueñas-Osorio L, Cimellaro G P. Uncovering the Heterogeneity of Spatial Lifeline System Interdependencies. *Proceedings of the 10th National Conference in Earthquake Engineering*, Earthquake Engineering Research Institute, Anchorage, AK, 2014.

interdependence damage propagation prediction model [2], with data obtained from the 2010 Chile earthquake was performed [3]. However, authors of these and related studies note that additional developments on network component fragility estimation and interdependence strength quantification are needed to further improve network vulnerability predictions, particularly for systems that include buried networks like water and gas, as well as for systems with not well understood coupling interfaces across them.

In fact, when assessing multi-network component fragility, an important factor to take into account, besides the fragility of components, is the *interdependence strength* between infrastructure system facilities. A time series approach [4] applied to restoration curves of infrastructures after the 2010 Chile earthquake was capable of estimating the interdependent coupling strengths between diverse networks at the city and regional levels and relate them to overall component or system-level functionality; other authors have recently adopted this methodology for different seismic events as well [5,6]. However, interdependence strength is variable across geographies, and thus a spatial focus to infrastructure systems is warranted besides their temporal aggregated effects. For instance, the Kriging Aided Spatial Correlation Algorithm (KASCA) [7]; is a recent methodology that analyzes the cross-correlation between network restoration patterns considering their actual spatial distribution. This approach provides insights on how multiple coupling locations and local features of the built environment affect interdependence, how influential coupling effects are as a function of distance, and how directionality effects could emerge from the multi-utility restoration patterns in space.

This paper performs a systematic exploration of spatial restoration processes on several coupled modern lifeline networks using restoration post-event data, and contributes to model development and sensitivity analyses from the application of ordinary point kriging to estimate spatial interdependence strengths of networks subjected to earthquakes. This spatial-based methodology is expanded at the local scale and applied for the first time to four lifeline networks, which were particularly affected by the 2010 Mw 8.8 Chile Earthquake. Results are then analyzed relative to field data and local features, as well as qualitatively compared to previous analyses involving related networks and metrics. Kriging interpolation has been used in many seismic hazard applications, such as earthquake hazard zoning in areas of Indonesia and Mexico [8,9]; however, KASCA is one of the emerging implementations for interdependence quantification efforts.

The remainder of this paper is structured as follows: The next section summarizes the mathematical concepts that underpin the proposed methodology for correlation coefficients derivation across networks via kriging surfaces. Then, we discuss the application of these concepts and strategies to derive spatial correlations in the context of the 2010 Chile earthquake for four lifeline systems, including power, water, fixed telephones and internet. Moreover, we discuss the results from the methodology presented in this paper as well as new insights of the spatial coupling analyses. Finally, we discuss the main conclusions from this study and directions for future research.

Mathematical Concepts for Spatial Correlation Analysis of Lifeline Interdependencies

Pearson's correlation coefficient has already been used as a measure of association to quantify the

degree of interdependence between infrastructure systems [10]. Pearson's coefficient ρ [11] describes the degree of linear correlation between two sets of data, and it is a generally accepted metric to quantify interdependence [4, 10, 12]. In this paper, ρ is used for the spatially distributed restoration potential data (time to restoration), denoted $\psi_{j,zi}$, with j taking the form of P, W, T and I referring to the Power, Water, Telephone and Internet systems, respectively, and Z_i indicating the location of point i in the horizontal plane. Hence, $\psi_{j,zi}$ values are spatially distributed points capturing restoration times from field data, which are then used to derive correlations across points between networks. In the context of network analysis, spatial correlations of datasets from the same network (e.g. $P \rightarrow P$) describe the auto-correlation, (which relates to intra-network dependency), while spatial correlations of datasets across different networks describe their cross-correlation (e.g. $P \rightarrow W$), which relates to inter-network dependency.

Before starting the spatial correlation analysis, it is necessary to construct kriging surfaces from $\psi_{j,zi}$ data to enable interpolation and interrogation of data values at particular spatial coordinates for interdependent correlation analysis. The kriging calculation first requires the formulation of a variogram, which describes the spatial dependency of observations in the sets containing $\psi_{j,zi}$ points. The process of estimating the variogram from sampled data is called variography. It begins with the calculation of the variogram estimator derived from the raw data [13]:

$$\gamma_E(h) = \frac{1}{2N(h)} \sum_{i=1}^{N(h)} (\psi_{j,zi} - \psi_{j,zi+h})^2 \qquad (1)$$

where $\psi_{j,zi}$ and $\psi_{j,zi+h}$ denote the restoration potential for a system j evaluated at points z_i and z_i+h and $N(h)$ describes the number of pairs of points within the lag interval h, taken to be the Euclidian distances between the two points i and $i+h$ and may be set equal to the mean minimum distance between pairs. The variogram model is a parametric curve fitted to the variogram estimator. Many models are available for this, including the spherical, exponential, and gaussian models [14]; however, some considerations must be accounted for when fitting models to the variogram estimator. Some preliminary guidelines derived from sensitivity analyses are proposed. When using Eq. 1, considerations applied in geostatistics are a good starting point; nevertheless, caution must be taken in regards to the lag size h. The size of the lag interval must be small enough to capture the evolution of the semi-variance (Eq. 1) at local scales, allowing the variogram model to present a well defined *range* and *sill*, where the first defines the maximum distance for which two $\psi_{j,zi}$ values are spatially correlated and the second approximates the variance of $\psi_{j,zi}$ values . Additionally, when modelling the variogram, one should not consider the nugget effect, which is the intercept with the ordinate, and has the potential to produce discontinuities on the kriging surface between sampled data and interpolated locations.

Ordinary point kriging (OPK) interpolates the $\psi_{j,zi}$ values at a particular point z_P by calculating the weighted average of $\psi_{j,zi}$ values evaluated at an N number of neighboring points. This interpolation is expressed in Eq. 2, where λ_i is the weighting coefficient associated with point z_i that must be estimated satisfying the constraints in Eqs. 3 and 4, while minimizing the mean-squared error in Eq. 5:

$$\hat{\psi}_{j,z_P} = \sum_i^N \lambda_i \psi_{j,z_i} \qquad (2)$$

$$\sum_i^N \lambda_i = 1 \tag{3}$$

$$E(\hat{\psi}_{j,z_P} - \psi_{j,z_P}) = 0 \tag{4}$$

$$E((\hat{\psi}_{j,z_P} - \psi_{j,z_P})^2) = 2\sum_{i=1}^N \lambda_i \gamma(z_i, z_P) - \sum_{i=1}^N \sum_{k=1}^N \lambda_i \lambda_k \gamma(z_i, z_k) \tag{5}$$

where $\psi_{j,zp}$ is the true but unknown value of ψ_j evaluated at a particular point z_P and $\gamma(z_i,z_k)$ is the variogram between values at zi and z_k. The optimization problem is solved using a Lagrange-multiplier v, resulting in a linear kriging system of $N+1$ equations. One equation is already expressed in Eq. 3, and the i^{th} equation of the remaining N becomes [15]:

$$\sum_{k=1}^N \lambda_k \gamma(z_i, z_k) + v = \gamma(z_i, z_P) \tag{6}$$

A simple illustrative example for spatial interpolation with ordinary point kriging is developed next. Fig. 1a depicts a slice of random correlated point processes varying in a two dimensional space that has been evaluated at some points in a 4×4 grid. Assume that an estimate of the random variable describing the field values is needed at the center. One can solve this problem applying the ordinary point kriging (OPK) interpolation method (Eq.1-6).

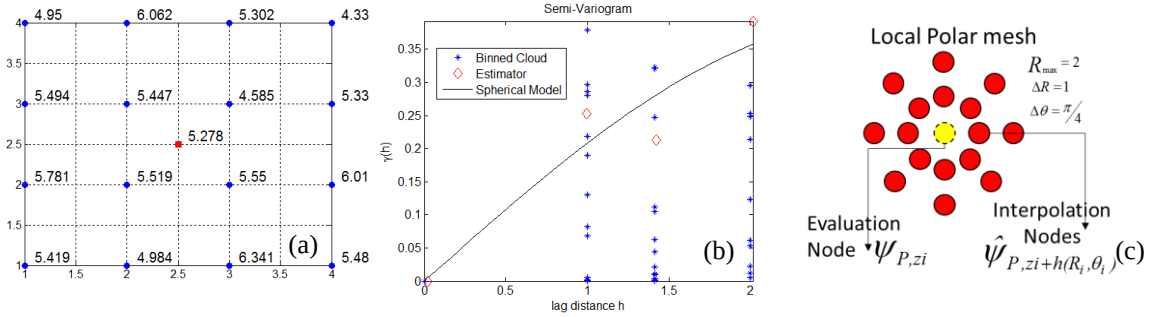

Figure 1. Interpolation set up for KASCA. (a) Evaluation and interpolation locations. (b) Graphical representation of the experimental variogram, estimator, and spherical model. (c) An example of a local polar mesh for a single sample location for network *P*.

The process starts with the variography. First, we compute all pairwise empirical semi-variances (Fig. 1b) . Then, adopting the common practice [15] of considering pairs separated by distances lower than a half of the maximum pair distance on the set and using a number of 20 intervals *h* (Eq. 1), as a fist tentative, we fix 20 bins of lag size *h* equal to *0.106*, and use Eq. 1 to compute the variogram estimator at each interval. Moreover, we fit several models to the averaged semi-variances deriving from the variogram estimator but decide to keep the spherical model (sill and range of *0.392* and *2.691* respectively) because it provides the best regression coefficient (Fig. 1b). The fitted model allows computing the semi-variances needed in Eq. 6 and solve for all λ_i and v, using Eq. 3 as well. Finally, using Eq. 2 the estimate at the center of the grid is $Z = 5.278$ (Fig. 1a). It should be noted that in this example a reduced population was considered; however, in applications, a greater population should be used, models should be adjusted through weighted

least-squares fitting [14], and varying the parameter of the estimator in Eq. 1 is always advisable in order to get better models of the spatial variability of the $\psi_{j,zi}$ values.

The spatial correlation analysis strategy for infrastructure data adopted in this paper starts at the local scale defining a polar mesh (Fig. 1c) around each evaluation node, referred to as the local mesh, where shifted estimates respect to $\psi_{j,zi}$ are computed using OPK. Then, co-located local sets of estimates pertaining to different networks are used to compute local correlations. Successively kriging the correlation estimates at sampled locations over the defined meshes *local correlation maps* are constructed. These maps quantify the degree of association between collocated restoration patterns. Also, we correlate all the set of $\psi_{j,zi}$ values at the evaluation nodes with the respective shifted estimates at relative positions $h(R_i,\theta_i)$. We represent a correlation coefficient for each set of pairs shifted and non shifted $\psi_{j,zi}$ values (interpolation and evaluation node respectively) in polar plots called *global correlation maps*, having the same structure of a local mesh (Fig. 1c) and we use them to study the anisotropy of spatial correlation. Finally, we average the correlation coefficients over the polar mesh (Fig. 1.c) in θ direction for all R_i to study the correlation range as function of distance and quantify the *length of interdependence*, being this a global average of the radius of influence of local recovery across systems. All previous maps and plots are going to be presented in the next section. In general, if both sets are referring to the same network *j* for the global analysis, intra-dependence coefficients are estimated; otherwise, the computed correlation coefficients depict inter-dependence between the respective networks.

Estimating Spatial Interdependence with Kriging Surfaces for Field Data

The kriging-based spatial correlation strategies from the previous section are applied for the first time to more than 2 systems, including power, water, telephone and internet network systems of the Talcahuano-Concepción area of Chile, in the context of the 27 February 2010 M_W 8.8 Offshore Maule earthquake. The restoration potential ψ_j of network *j* takes the form of days of repair to service full restoration, which is the field collected post-event data at a number *N* of locations (evaluation nodes). For the power and water networks $N = 94$, while for the telephone and internet networks $N = 70$.

Spatial correlation analyses require kriging surfaces to include values at additional coordinates $z_i + h(R_i,\theta_i)$, describing various *R* Euclidian distances from each evaluation node at coordinates (z_i), with varying θ angles in the horizontal plane. Thus, a mesh of $z_i + h(R_i,\theta_i)$ coordinates is created using distance increments ΔR of 125 m up to a maximum distance *R* of 2.5 km and angle increments $\Delta\theta$ of $\pi/20$ in the horizontal plane. Kriging surfaces of $\psi_{j,zi}$ values are derived within this mesh for each network. The local mesh parameters are not known beforehand, however, a good start for the radius *R* is one fourth of the maximum pair distance of evaluation nodes and the number of increments in directions R and θ can be set to 20. After running KASCA for the first time on field data, one can increase resolution with more increments to make the maps and plots smoother and not miss local features or reduce resolution using fewer increments to reduce the computational cost. The resulting kriging surfaces (Fig. 2) are presented as a cloud of points describing the value of $\psi_{j,z}$ at those points.

Computing the local correlation between the $\psi_{j,z}$ values in a local mesh with the $\psi_{k,z}$ values of

another network in a co-located mesh results into a correlation value located at the evaluation node (center of co-located polar meshes). Repeating this process for all local meshes and successively kriging the correlation estimates leads to the local correlation maps in Fig. 3, which depict the rich spatial heterogeneity in restoration interdependence; more details are discussed in the next section. Then, global correlation analysis is pursued to synthesize local trends. Consider set X as all evaluation nodes in network j and set Y as all interpolated nodes in network k, but shifted by a distance R_P and a direction θ_P from the center of the local meshes (an evaluation node) in accordance to the established radial and angular increments of the local mesh. Then, we correlate the sets and locate that correlation coefficient in a polar grid with coordinates R_P and θ_P. By repeating this process, fixing set X as reference and varying set Y for all ΔR and $\Delta\theta$ increments from 0 to $2.5km$ and from 0 to 2π respectively, yields to a global correlation map between two networks (Figs. 4 and 5). Finally, averaging the previous results in the θ direction allows studying spatial correlation as a function of distance only. The error bars in Fig. 6 depict one standard deviation from the mean. All these results are studied next.

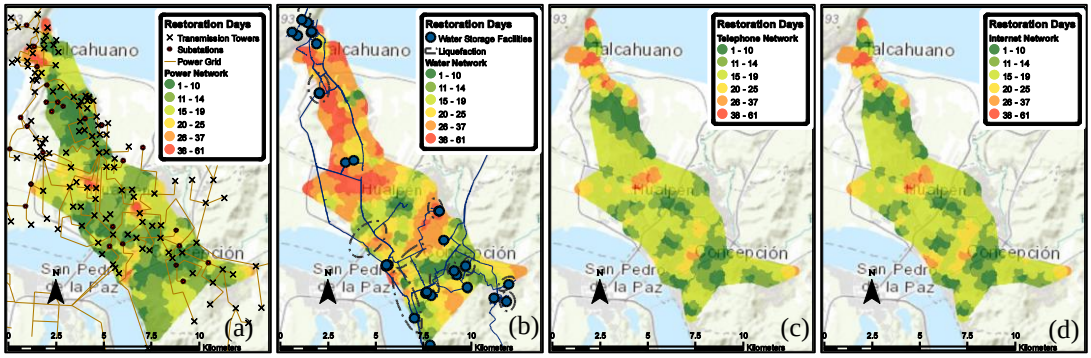

Figure 2. Restoration potential $\psi_{j,z}$ expressed in days of repair to service full restoration for the (a) power, (b) water, (c) telephone, and (d) internet networks.

Analysis of KASCA Results

The kriging surface in Fig. 2a representing the power network restoration shows that most of the recovering finished within 15 days after the event; peaks in the surface represent major delays matching the locations of electrical substations and transmission lines that could have been particularly affected by the earthquake. In addition, the water network restoration surface (Fig. 2b) indicates that the recovering started at the south part of the studied area, where the water treatment plant intake is located, and continued towards the north presenting major delays exceeding 38 days after the event. Similarly, peaks out of the trend of the restoration scheme match zones in which liquefaction was verified. In relation to the recovering of the telephone and internet networks (Fig. 2c-d), both surfaces are quite similar, supporting the fact that they share similar infrastructure; also, the surfaces seem to be delayed with respect to the power network restoration surface, confirming the great impact that the power outage had in the telecommunication network systems [16]. Also, most of telecommunication systems' functionality was recovered in less than 20 days after the event.

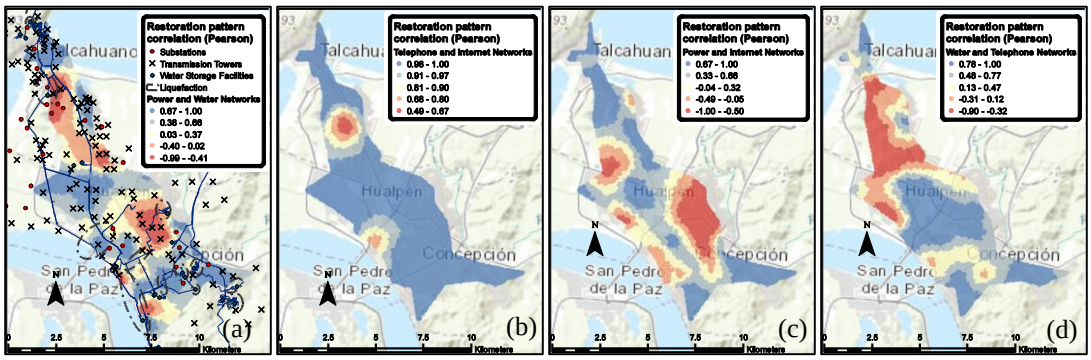

Figure 3. Local correlation maps between (a) power and water ($P \rightarrow W$), (b) telephone and internet ($T \rightarrow I$), (c) power and internet ($P \rightarrow I$), and (d) water and telephone networks ($W \rightarrow T$).

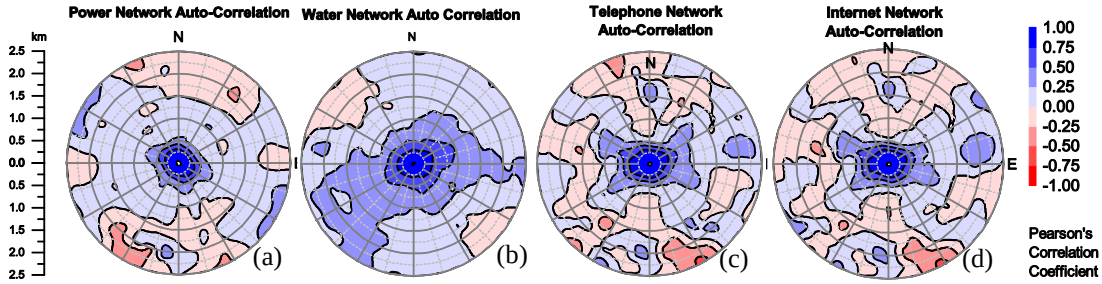

Figure 4. Global spatial autocorrelation maps of the (a) power, (b) water, (c) telephone, and (d) internet networks.

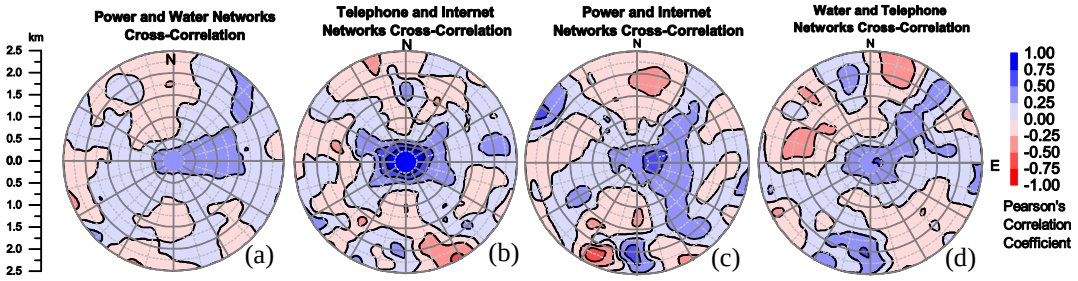

Figure 5. Global spatial cross-correlation maps between (a) power and water ($P \rightarrow W$), (b) telephone and internet ($T \rightarrow I$), (c) power and internet ($P \rightarrow I$), and (d) water and telephone networks ($W \rightarrow T$).

The local correlation maps in Fig. 3 captured the interdependent behavior across the lifeline systems, where the positive correlation means a favored or simultaneous progress in restoration across systems, and the negative correlation is interpreted as progress of one system and stagnation of the other. Fig. 3a suggests delays in the recovery of the water network with respect to the power network in some areas, which is particularly the case for the arcs of the water network surrounding the water treatment plant. They also captured (Fig. 3b) the simultaneous loss of connectivity between the telecommunication services and the central offices by presenting a uniform distribution of high correlation values across the region. The interaction between the power and

internet network (Fig. 3c) was not as uniform as expected, because of the damages in the specific components of the telecommunication and the power network, however, they hold that the restoration progress tend to be similar across system in a range of 1-2 kilometers diameter. The local correlation map in Fig. 3.d depicted assistance from the telephone network to the water network restoration logistics and the diameter of the range of correlation seems to be greater than 2 kilometer for some components.

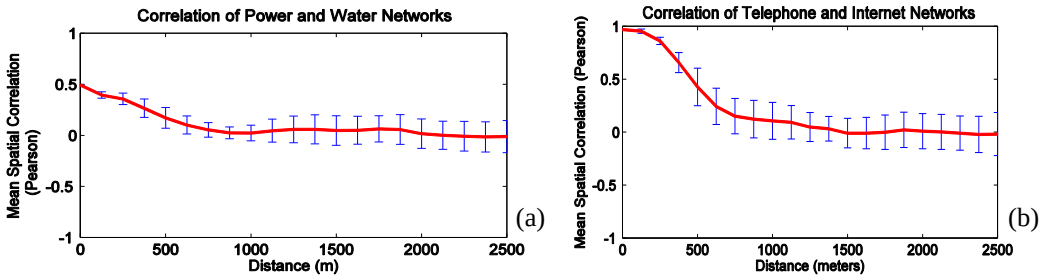

Figure 6. Global averaged correlation plots. (a) Cross-correlation plot between the power and water network. (b) Average correlation plot between the telecommunication networks.

The global correlation maps in Fig. 4 and 5, present overall high correlation towards the center, while correlation generally decreases as the distance from the center increases. For the autocorrelation its value is exactly 1 at the center but when cross-correlations are computed the value at the center can be interpreted as the global coupling strength of co-located lifeline systems. However, it can be observed that for all plots the correlations are not radially symmetric. Global auto-correlation maps for the water network (Fig. 4b) demonstrate that towards the north and south, matching the geometry of the pipelines crossing Talcahuano and Concepción areas (Fig. 2b), the correlation practically vanishes, but towards the east and west it does not vanish completely. This suggest that the restoration of the water network facilities granted functionality to adjacent facilities towards the east and west from the pipelines but until the labors of restoration from liquefaction and other site effects in the main pipelines are not progressing towards the north, northern facilities and users are not gaining functionality. Fig. 5a depicts favored coupling between the power and water systems towards the east, meaning that there is a large interdependent area in which water facilities are being supplied with electricity from service areas within distances reaching 1.5 kilometers. The global correlation map in Fig. 5b referring to the telecommunication networks indicates that the directionality was not as imperative as distance in the interdependence phenomenon. The restoration pattern of the power network aided the internet networks to recover towards the east (Fig. 5c), indicating supplying of electricity at great distances in this direction. Finally, the global correlation map integrating the water and telephone networks (Fig. 5d) depicts support from the telecommunication network in the repair efforts of the water network towards the north-east and west for logistics and coordination efforts.

In relation to the global averaged correlation plots in Fig. 6, their correlation vanishes after approximately 1.5 kilometers, meaning that interdependence effects on restoration tend to be localized given the overall damage across entire systems. Regarding the different shapes of the curves, the telecommunication stays constant and then decreases suddenly after around 200 meters,

while the power and water networks present a linear decreasing trend of the coupling behavior. This could be explained by the fact that the telecommunication networks do not operate in a fixed topology and its components are connected wirelessly within a certain range of coverage, but once exceeded this range, the association of systems restoration involves more components performing diversely, decreasing the correlation estimates for small increments of distance. In contrast, the power and water network are constrained to their physical layout and present physical connections at closer distances that affect the correlation estimates progressively along the influence length. In addition, the telephone and internet networks presented the highest coupling strengths; this is explained after realizing that both networks are using digital technology, and then, both services could be connected to the same central offices in which their equipment was affected by the event.

Conclusions

This paper expanded the kriging aided spatial correlation algorithm (KASCA) [6], by introducing guidelines for the formulation of the kriging surfaces and deriving local correlation maps, global correlation maps and averaged correlation plots for a larger number of coupled lifeline systems. The enhanced approach was applied for the first time to several lifeline systems, including power, water, telephone, and internet lifeline systems during the 2010 Mw 8.8 Chile Earthquake to capture interdependence strength, directionality and length.

The kriging surfaces resulting from this methodology provide a realistic estimate of lifelines performance by matching available actual responses. Also, local correlation maps are able to establish interdependence estimates between networks and their components, and when not possible, they point out aggregated effects due to adopted repair schemes or local effects, such as liquefaction damages to buried networks. Global correlation maps verified directionality of the coupling in restoration between networks for the water and power network, and a less anisotropic behavior for the telecommunication networks. Averaged correlation plots provided estimates referring to the length of interdependence influence of around 1.5 kilometers and coupling strengths for all pairwise networks of 0.494, 0.554 , 0.502, 0.504, 0.471 and 0.969 ($P \rightarrow W$, $P \rightarrow T$, $P \rightarrow I$, $W \rightarrow T$, $W \rightarrow I$ and $T \rightarrow I$, respectively). These correlation values compare adequately to results obtained in similar analyses, which were limited to the same water and power networks aggregated at regional and city levels [4].

The applied methodology provides simulation models that yield realistic coupling strengths and influence lengths considering the relative position of network facilities. When using real time data this method not only can help calibrate models of interdependence but also aid decision making. For instance, global autocorrelation maps can identify directions in which restoration efforts are not having impact in the overall restoration of a network or directions in which the level of damage was more severe to identify broken connections or change direction of repair scheme to optimize restoration. Global crosscorrelation maps can indicate until which spatial extent restoring a network is assisting other network so extra resources can be allocated as needed. Global autocorrelation and crosscorrelation plots provide a length of correlation that can help selecting the size of the backups, crews and material resources.

Future research should aim to integrate the network topological information and the state of

restoration at varying points in time, as found in time series correlation approaches [4], but for every point in space for a joint spatial-temporal description of interdependence. This would particularize the correlation estimates towards the specific component level of detail, quantifying for each of them the interdependence among components pertaining or not to the same network, their directionality, and length of influence.

Acknowledgments

The second author would like to acknowledge partial support from the U.S. National Science Foundation through grant CMMI-0748231 and the U.S. Department of Defense's Army Research Office through grant W911NF-13-1-0340. Any opinions, findings and conclusions or recommendations expressed in this work are those of the authors and do not necessarily reflect the views of the sponsors. The authors also would like to thank Dr. Mauricio Villagrán for his support with data collection and technical discussions, as well as to Jason Wu for his initial developments of KASCA.

References

[1] Bonneau, A. and O'Rourke, T.D. Water Supply Performance during Earthquakes and Extreme Events. MCEER, University at Buffalo. Buffalo, New York, 2009.
[2] Hernandez-Fajardo, I., and Dueñas-Osorio, L. Sequential Propagation of Seismic Fragility across Interdependent Lifeline Systems. *Earthquake Spectra*. 2011; **27**: 23-43.
[3] Wu J, Dueñas-Osorio L. Calibration and Validation of a Seismic Damage Propagation Model for Interdependent Infrastructure Systems. *Earthquake Spectra*. 2013; **29** (3):1021–1041.
[4] Dueñas-Osorio L, Kwasinski A. Quantification of Lifeline System Interdependencies after the 27 February 2010 M_w 8.8 Offshore Maule, Chile, Earthquake. *Earthquake Spectra*. 2012; **28**: 581-603.
[5] Cimellaro GP, Solari D, Renschler CS, Reinhorn AM. Community resilience index integrating network interdependencies. *Structures Congress.* 2013: 1789-1799.
[6]. Cimellaro GP, Solari D, Bruneau M. Physical infrastructure interdependency and regional resilience index after the 2011 Tohoku Earthquake in Japan. *Earthquake Engineering & Structural Dynamics*. 2014. Advance online publication. doi:10.1002/eqe.2422.
[7] Wu J, Dueñas-Osorio L. Spatial Quantification of Lifeline System Interdependencies. *Proceedings of the 15th World Conference on Earthquake Engineering*. Lisbon, Portugal, 2012.
[8] Irwansyah E, Winarko E, Rasjid ZE, Bekti RD. Earthquake hazard zonation using peak ground acceleration (PGA) approach. *Journal of Physics: Conference. Series*. 2013; **423**: 012-067.
[9] Osorio L, Mayoral JM. Seismic microzonation for the northeast Texcoco lake area, Mexico. *Soil Dynamics and Earthquake Engineering*. 2013; **48**: 252–266.
[10] Mendonça D, Wallace WA. Impacts of the 2001 World Trade Center Attack on New York City Critical Infrastructures. *Journal of Infrastructure Systems*. 2006; **12**: 260–270.
[11] Rodgers J., Nicewander W. Thirteen Ways to Look at the Correlation Coefficient. The American Statistician 1988; **42**: 59 – 66.
[12] Kendall, M. and Gibbons, J.D. Rank Correlation Methods. *5th ed. Oxford University Press*. New York, 1990.
[13] Matheron G. *Les Variables Régionalisées et leur Estimation*. Masson. Paris, 1965.
[14] Oliver M., Webster R. A tutorial guide to geostatistics, computing and modelling variograms and kriging. *Catena.* 2014; **113**: 56–69.
[15] Trauth M. *Matlab Recipes for Earth Sciences*. Springer. Meppel, 2007.
[16] Technical Council on Lifeline Earthquake Engineering. *Chile Earthquake of 2010: Lifeline Performance*. Monograph Series N° 36. United States of America. 2013.